Sub-Severe and Severe Hail

KIMBERLY L. ELMORE,[a,b] JOHN T. ALLEN,[c] AND ALAN E. GERARD[b]

[a] *Cooperative Institute for Severe and High-Impact Weather Research and Operations, University of Oklahoma, Norman, Oklahoma*
[b] *NOAA/National Severe Storms Laboratory, Norman, Oklahoma*
[c] *Department of Earth and Atmospheric Sciences, Central Michigan University, Mt. Pleasant, Michigan*

(Manuscript received 27 September 2021, in final form 3 May 2022)

ABSTRACT: The occurrence and properties of hail smaller than severe thresholds (diameter < 25 mm) are poorly understood. Prior climatological hail studies have predominantly focused on large or severe hail (diameter at least 25 mm or 1 in.). Through use of data from the Meteorological Phenomena Identification Near the Ground project, *Storm Data*, and the Community Collaborative Rain, Hail and Snow Network the occurrence and characteristics of both severe and sub-severe hail are explored. Spatial distributions of days with the different classes of hail are developed on an annual and seasonal basis for the period 2013–20. Annually, there are several hail-day maxima that do not follow the maxima of severe hail: the peak is broadly centered over Oklahoma (about 28 days yr^{-1}). A secondary maximum exists over the Colorado Front Range (about 26 days yr^{-1}), a third extends across northern Indiana from the southern tip of Lake Michigan (about 24 days yr^{-1} with hail), and a fourth area is centered over the corners of southwest North Carolina, northwest South Carolina, and the northeast tip of Georgia. Each of these maxima in hail days are driven by sub-severe hail. While similar patterns of severe hail have been previously documented, this is the first clear documentation of sub-severe hail patterns since the early 1990s. Analysis of the hail size distribution suggests that to capture the overall hail risk, each of the datasets provide a complimentary data source.

KEYWORDS: Atmosphere; North America; Hail; Thunderstorms; Climatology; Databases; Sampling; Statistical techniques; Agriculture; Insurance

1. Introduction

In the United States, hail size is divided into two classes: severe, meaning a diameter of at least 25 mm (1 in.) and sub-severe, meaning anything less than 25-mm diameter, but greater than the 5-mm diameter of graupel (Allen et al. 2020). These two size classes are used to define whether the event meets severe criteria. Prior to January 2010, the severe class was defined as hail with a diameter at least 19 mm (0.75 in.). The overall occurrence of hail has been regularly explored in the United States given its substantive and rising impacts to both property and agriculture; however, how frequently smaller hail sizes occur has received less attention (Changnon 1999; Sander et al. 2013; Brown et al. 2015; Tang et al. 2019; Allen et al. 2020). Inferring the occurrence of hail is challenging owing to the spatial and temporal inhomogeneities that arise from typical observer-sourced datasets used to validate severe thunderstorm warnings (i.e., SPC *Storm Data*; Kelly et al. 1985; Schaefer et al. 2004; Doswell et al. 2005; Allen and Tippett 2015; Allen et al. 2017; Taszarek et al. 2020). The relationship of these data to warning verification (Blair et al. 2011; Bunkers et al. 2020) means that size criteria within the dataset are mostly confined to no less than 19 mm (0.75 in.) for hail and so sizes smaller than 19 mm are poorly represented. Smaller sizes are occasionally included if they are associated with severe wind, or a tornado. As noted by Changnon (1999), this limits the utility of these data in describing the true hail frequency, or the full distribution of hail sizes that occur. Only about the last two decades contain reliable hail data (Allen and Tippett 2015) meaning that prior to the 1990, these data are rarely used because they lacked the necessary consistency to ascertain the true frequency of hail of any size in the United States (Changnon 1999). Instead, prior studies relied either on station-based observations (Changnon 1977a,b; Changnon and Changnon 1997, 2000; Changnon et al. 2001, 2009), hail pads, or agricultural damage data to infer these events. While these past datasets for the most part still exist for assessment of hail occurrence, station-based observations have only had size information for brief periods and formal observations were terminated in the 1990s. Hail pad records have generally been inconsistent in their maintenance or heavily regionalized (e.g., Reges et al. 2016), seriously limiting any climatological utility.

The limitations of *Storm Data* have spurred newer approaches that are more dynamic and widespread to collect precipitation data including hail. For example, the CoCoRAHS observation network collects more detailed hail information through either hail pads or spotter observations and includes each of the smallest, average, and largest size of hail along with other properties (Reges et al. 2016). Other high density observation collection efforts include the Severe Hazards and Analysis and Verification Experiment (SHAVE; Ortega et al. 2009; Ortega 2018), which actively probed areas around strong storms in near–real time to obtain observations to verify temporal and spatial scales of hail for the verification of radar derived hail products. While an effective approach to collate hail events, it was

Supplemental information related to this paper is available at the Journals Online website: https://doi.org/10.1175/WAF-D-21-0156.s1.

Corresponding author: Kimberly L. Elmore, kim.elmore@noaa.gov

DOI: 10.1175/WAF-D-21-0156.1

limited in coverage, and by the available personnel to make calls at any given time. Despite these limitations, SHAVE documented otherwise unprecedented unknown scales of hail fall and size on a comparatively large sample of storms. In parallel there have also been small scale efforts to source high density measurements in the field, and while they have also contributed to our understanding of hailstone and hail fall properties, their records are too sporadic to contribute to the climatological understanding (Blair et al. 2017; Giammanco et al. 2017).

A more accessible and easily managed approach to collating hail information has been through the Meteorological Phenomena Identification Near the Ground (mPING) project that implements a flexible Application Program Interface on a mobile phone platform to crowdsource volunteer reports of precipitation events (Elmore et al. 2014). As a result of these efforts, the mPING project has garnered an impressively large collection of hail events in the past 8 years across the continental United States, ranging from 6.35 mm (0.25 in.) maximum diameter through sizes in excess of 125 mm (5 in.). By approaching the problem through this platform, mPING provides valuable insight into the hail sizes that are not traditionally collected or sought by existing approaches. Despite these favorable attributes, to date data from mPING have not been used in a climatological context, and small hail climatology over the United States has not been explored since 2005 (Changnon et al. 2009).

While a number of studies have explored the individual datasets that characterize hail occurrence (e.g., Changnon 1999; Doswell et al. 2005; Changnon et al. 2009; Allen and Tippett 2015; Grieser and Hill 2019), no effort has been made to explore a more comprehensive picture of hail occurrence through the synthesis of multiple observational datasets to leverage their relative strengths and address their weaknesses. This limitation to existing approaches has only been emphasized since the retirement of detailed hail reporting from station observations (Changnon 1999), leading to an incomplete picture of hail day occurrence for the full distribution of hail sizes. Understanding the climatology of all hail is important as sub-severe hail can lead to significant agricultural damage (Changnon 1971; Changnon and Changnon 1997), and if accumulated can result in dangerous road conditions and localized flash flooding (Kumjian et al. 2019; Friedrich et al. 2019). In some regions and seasons, these smaller hail sizes can be the primary mode of occurrence (e.g., Miller and Mote 2017), and can provide important insights into ice processes of strong convective clouds (Van Den Heever and Cotton 2004; Kacan and Lebo 2019). The analysis of the spatial distribution of all hail sizes is also essential for the cross-validation of proxy hail climatologies that are derived through the use of remotely sensed satellite and radar platforms (e.g., Cintineo et al. 2012; Cecil and Blankenship 2012; Bang and Cecil 2019; Murillo et al. 2021; Wendt and Jirak 2021). For example, using only SPC storm reports to validate these measurements, it is not clear whether the radar-derived frequencies indicated from maximum expected size of hail detections (MESH; Murillo et al. 2021; Wendt and Jirak 2021) were an overestimate of hail frequency, or an overestimate of hail sizes or perhaps a combination of both. To this end, in this paper we consider climatological frequency and bulk statistics of hail as ascertained from the combination of mPING, *Storm Data*, and CoCoRaHS and explore the relative strengths and weaknesses of each dataset. The aim of this work is to produce a comprehensive climatology of hail in the contiguous Unites States and, in so doing, recognize unique strengths and weaknesses of each data source and the information provided through their cumulative hail observations.

2. Data and methods

Data used in computing hail days for sub-severe and severe hail come from two sources: the National Oceanic and Atmospheric Administration/National Centers for Environmental Information (NOAA/NCEI) *Storm Data* publication and mPING. These two sources differ substantially in that *Storm Data* is primarily used for NWS warning and verification purposes. This means that offices actively probe for relevant reports in areas of suspected severe weather, and reporting in the vicinity of NWS offices involves a higher fraction of NWS Employee reports (Allen and Tippett 2015). Reports are entered as the nearest reference object identified by the user or NWS employee entering the report. In contrast, mPING is a passive collection of voluntarily provided reports provided by mPING users. Unlike *Storm Data*, users are also provided a referential list of hail sizes at quarter inch intervals and associated reference objects, which may assist in mediating size clustering bias toward known reference objects (Allen and Tippett 2015; Blair et al. 2017). The period of record for mPING considered here spans 8 years from 1 January 2013 to 31 December 2020; however, mPING remains operational. All data used in this analysis appear in the online supplemental content. These data include UTC time of the observation, latitude, longitude, and hail diameter.

The nature of mPING observations means that they are automatically located in space and time by GPS and are thus spatially more accurate than other sources of reports, unless a user moves a considerable distance from the observation or waits a long time to send the report; cursory examination shows no evidence of such. No quality control is performed to mPING hail observations, outside of truly erroneous submissions, though no systematic biases that would influence the study results are present to the authors' knowledge. *Storm Data* does not enjoy such precision and while *Storm Data* errors have been well documented (e.g., Witt et al. 1998) here we take several steps to address these potential sources of error on the derived climatology. One area that cannot be remedied is the serious bias in hail size reports as sub-severe hail is not generally recorded except in cases where it may be in association with another type of significant weather (winds, tornadoes, etc.). In contrast, mPING encourages reports of sub-severe hail and so is the only available data source for a more general all hail climatology. Both sources suffer from a spatial bias in that reports are naturally more numerous in and around population centers and road networks (Allen and Tippett 2015). Without care, this can lead to misleading conclusions related to the association of high frequency hail with high population density.

To illustrate these potential biases in the two datasets and the distinct difference in the raw frequency of reports, we consider both sub-severe (Figs. 1a,b) and severe (Figs. 2a,b) point

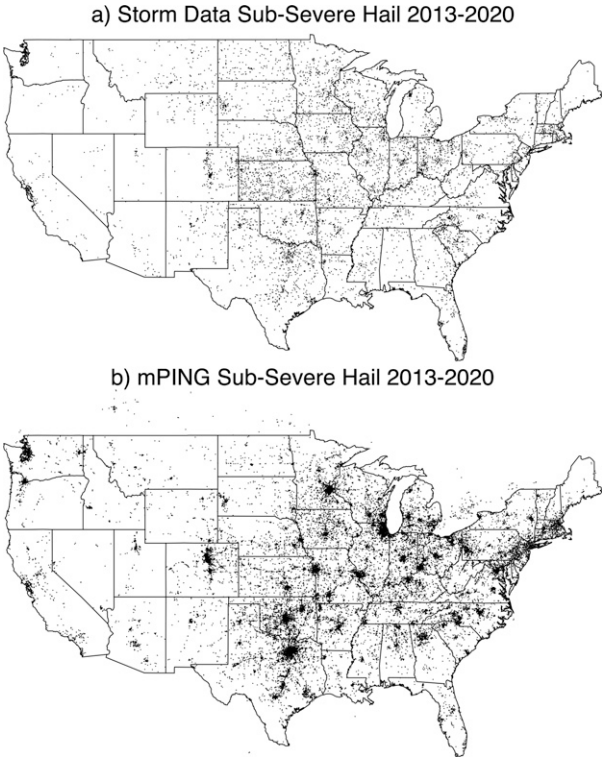

FIG. 1. (a) Point cloud showing *Storm Data* reports of sub-severe hail spanning the period 1 Jan 2013–31 Dec 2020; each point represents the location of a single *Storm Data* report. (b) As in (a), but showing sub-severe reports from mPING.

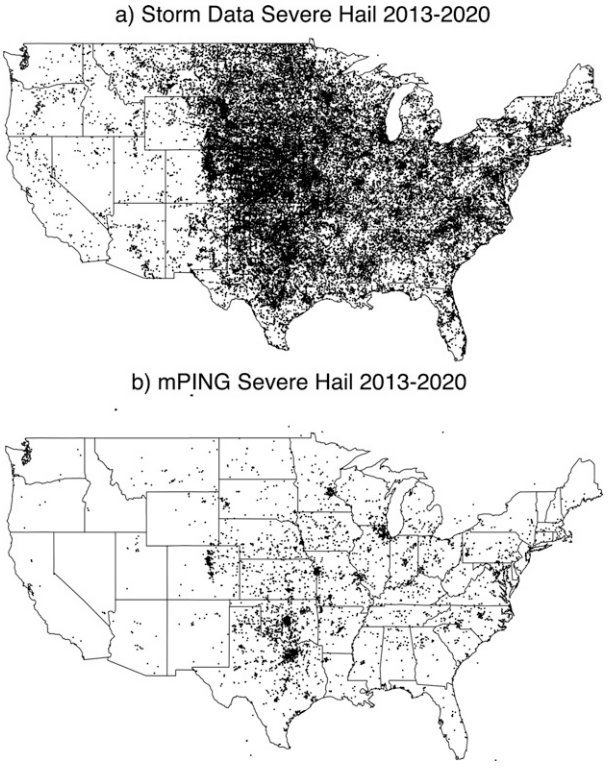

FIG. 2. (a) Point cloud showing *Storm Data* reports of severe hail, as in Fig. 1a. (b) As in (a), but for mPING reports of severe hail.

clouds from *Storm Data* and mPING, respectively. In both figures, areas of higher report density are clearly associated with cities and metropolitan areas in hail prone regions. Such density variations are nonphysical artifacts and therefore must be removed to the extent possible.

One approach to diminishing these population derived artifacts is through an analysis procedure that diffuses, filters, or "spreads out" this dependence over an appropriate area, an approach that has been used in numerous studies (e.g., Brooks et al. 2003; Gensini et al. 2020). Approaches such as Schaefer et al. (2004) treat this by aggregating (binning) *Storm Data* severe hail reports into 2° squares, averaging across the squares, then normalizing the results to reports per decade per 34 300 km^2 (10 000 n mi^2). Hexagonal binning (Carr et al. 1992) is another way to deal with this effect that has advantages over rectangular binning and therefore is the approach used here. Chiefly, hexagons are the most complex polygon that can be tessellated over a surface and are more similar to circles than are squares. Thus, hexagons and hexagonal binning constitute the most efficient and compact division of 2D data space. This property helps reduce the edge and border effects inherent in rectangular binning procedures.

For this work, a grid of 23 × 23 hexagons is distributed over the CONUS, providing for 529 center points. From this set, not all hexagons have hail observations as illustrated in Fig. 3. We experimented with the maximum number of hexagons and found that the aforementioned grid provided was the highest resolution that could be used before population centers began to clearly influence results. Each hexagon includes an area of about 32 600 km^2 (roughly equivalent to a 100 km radius circle). This area reflects a similar scale to that of Schaefer et al. (2004), thereby allowing for more direct comparison despite the different gridding approach.

To calculate the number of days with hail, reports from either dataset are binned within each hexagon; each day is counted only once. This step is critical to ensure that if there are many reports within a hexagon for a given date, that day is counted

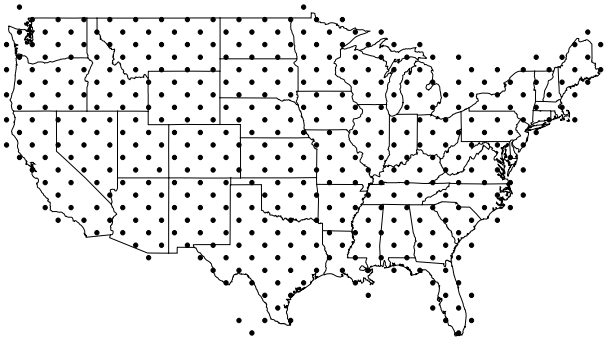

FIG. 3. Points showing the center of hexagonal cells that contain reports from either *Storm Data* or mPING over the period 1 Jan 2013–31 Dec 2002.

only once. Because the period of record covers 8 years, the total number of days is divided by a factor of 8 to yield the average number of hail days per year.

To smooth the results from the original hexagonal grid, a local, quadratic least squares surface is fit to the resulting grid of counts as an additional smoothing step (LOESS; Cleveland 1979; Cleveland and Devlin 1988). The resulting fit is applied to a finer grid for plotting purposes, and then used as the basis for contours of days per year of sub-severe hail, severe hail, or any hail.

Storm Data timestamps have known inaccuracies and tend to be biased late (after the event), yet *Storm Data* report time errors seldom exceed 1 h (Witt et al. 1998). Provided that mPING users submit reports during or very shortly after an event, mPING reports have reduced time errors relative to *Storm Data*. Times from both source datasets are used to generate distributions of event times, in local standard time (LST), to evaluate the most common time of day for hail events and to discern whether any difference exists between times by season or hail size. Occurrence time distributions are then estimated using kernel density estimates (KDEs) computed at 201 points each using a Gaussian weighting 12.7 mm wide (0.5 in.) truncated at four standard deviations (Silverman 1998).

Finally, a third data source reflecting the next largest available dataset was also considered, the Community Collaborative Rain, Hail and Snow Network (CoCoRaHS; Reges et al. 2016). As time information from CoCoRaHS is unreliable and difficult to ascertain, we instead focus on its application for understanding hail size distributions. We use CoCoRaHS to help generate distributions of hail size and estimate the proportions of sub-severe and severe or larger hail. For this application the use of both CoCoRaHS and mPING allows for a more comprehensive viewpoint of sub-severe hail, as *Storm Data* does not provide sufficient data of this type. The resulting distributions are created through empirical cumulative density functions (eCDFs).

3. Results

a. Sub-severe and severe hail frequency

Here we compare and contrast both the common and complimentary qualities of *Storm Data* and mPING for severe and sub-severe hail days. Unsurprisingly, there is a much larger fraction of sub-severe reports within mPING, and severe or greater reports in *Storm Data* (Figs. 1 and 2), suggesting that these two datasets are likely complementary by providing insight into different sizes of hail, rather than one being notionally superior to the other. Following gridding and smoothing to the annual average number of hail days of any size, Fig. 4 shows an estimate of the average total number of days with any hail across the CONUS as estimated using *Storm Data* (red) and mPING (blue). This approach further illustrates the differences between the two datasets because any hail frequency illustrates regions where hail less than an arbitrary threshold often occurs. This is particularly evident over the western United States where larger hail sizes are comparatively rare (Schaefer et al. 2004; Allen and Tippett 2015). Higher

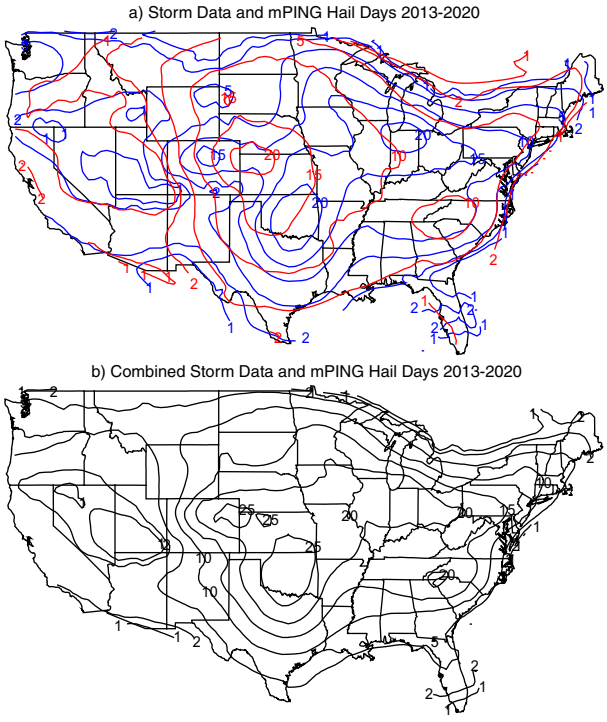

FIG. 4. (a) Contours of the average number of hail days per year for hail of any size from *Storm Data* (red) and mPING (blue). (b) As in (a), but for combined *Storm Data* and mPING reports.

frequencies are particularly evident outside of the typical Great Plains severe hail maxima, with higher frequency on and near the foothills of the Rocky Mountains, over the Midwest and East. Combining the two datasets, however, provides a complementary picture of the total number of hail days. We expect that the values in Fig. 4b provide the most accurate representation of average yearly hail days across the CONUS. These values are more broadly consistent than long term hail data records based on station data, though with some differences, including slightly higher frequencies reflecting the broader spatial sampling (Changnon and Changnon 2000). For example, Changnon and Changnon (2000) reported a hail day frequency of ~21 for Denver, Colorado, and Dodge City, Kansas, with a gradient through eastern Kansas. However, over regions with more sparse population, the reliability of observation stations overshadows this benefit. It is important to note that these sources are not exclusive or independent: a day that counts as a sub-severe hail day may also count as a severe hail day and vice versa. This explains why Fig. 4b is not simply the simple sum of occurrences within *Storm Data* and mPING.

Spatially, the overall patterns are similar to Schaefer et al. (2004); however, we note that study provides contours in number of *reports* per 10 years and thus the results are not directly comparable. The overall frequency of that study also depicts a maximum number of reports to be nearly 60 yr^{-1} for hail exceeding 0.75 in. This number is well in excess of the ~30 yr^{-1} for any hail size shown in Fig. 4b, reflecting the difference obtained if an approach uses hail *days* rather than hail

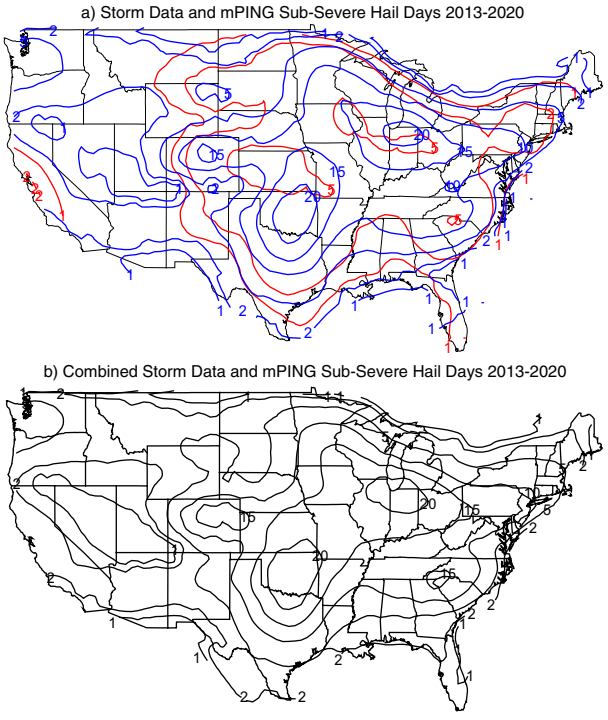

FIG. 5. (a) Contours of the average number of hail days per year for hail of sub-severe size from *Storm Data* (red) and mPING (blue). (b) As in (a), but for combined reports from both *Storm Data* and mPING.

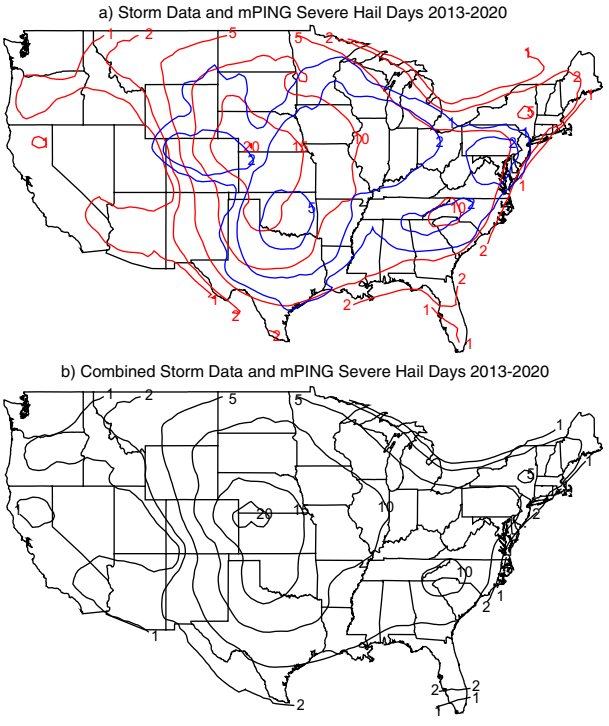

FIG. 6. (a) As in Fig. 5a, but for severe hail. (b) As in Fig. 5b, but for severe hail.

reports (Doswell et al. 2005; Allen and Tippett 2015). For this reason, in this work any single day that receives $n > 1$ reports still counts as a single day within a hexagonal bin.

Sub-dividing these reports into mean sub-severe days per year only, the differences between the two datasets are further emphasized (Figs. 5a,b). *Storm Data* shows two maxima, one of 6–7 days yr^{-1} across northwest Kansas and another near Charlotte, North Carolina. However, this is clearly an underrepresentation of the true frequency, as mPING shows what is almost certainly a more accurate depiction of sub-severe hail days because mPING is not, by design, biased toward severe hail. The most significant differences are in regions outside the traditional "hail belt," with maxima in the Colorado Front Range, central Oklahoma, and also an east–west region encompassing parts of the lower Midwest, as well as Kentucky, North Carolina, South Carolina, Georgia, and northeast Alabama. Curiously, the frequency of mPING reports also introduce spatial inhomogeneities; for example, *Storm Data* reports are more likely across the California seaboard as compared to those from mPING. In combining the two datasets (Fig. 5b), these reports show a pattern with clear maxima (24 days) over central Oklahoma, a northeast–southwest band from southern Wisconsin into northern Ohio touching the southern tip of Lake Michigan (18–24 days), a clear separate maximum along the front range of the Rocky mountains extending into eastern Colorado (16 days), and finally a fourth maximum encompassing eastern Kentucky, the southwest corner of North Carolina, the northwest corner of South Carolina, northern Alabama, and northern Mississippi (14–16 days). The maximum in central Oklahoma is part of a general ridge of high sub-severe hail frequency that extends into the Great Lakes region.

The patterns for severe hail (Figs. 6a,b) are decidedly different from sub-severe hail, and while spatially consistent are higher in frequency than the hail day rate reported using *Storm Data* alone (Allen and Tippett 2015), likely reflecting continual growth in hail reporting frequency. *Storm Data* shows a maximum of 20 days at the junction of Nebraska–Kansas–Colorado, along with a broader region of active severe hail days extending into western North Carolina. mPING does not record as many severe weather days, particularly outside of the traditional region for large hail east of the Rocky Mountains, with a maximum of only 6 days over central Oklahoma and a ridge of activity extending into the Great Lakes region, a broad east–west region over northern Colorado with a weak max roughly over Denver, Colorado, then a ridge centered roughly over the Appalachians. Through the merger of both sources (Fig. 6b), a more complete picture develops again highlighting their complementary nature. The 20-day maximum over the Nebraska–Kansas–Colorado intersection expands, with a clear ridge of frequency extending southeast into western Oklahoma and the eastern Texas Panhandle. The ridge of severe hail days remains over the Appalachians but likely has a true frequency closer to 8–10 days per year. These patterns are reminiscent of prior climatologies of hail day frequency (Doswell et al. 2005; Allen and Tippett 2015);

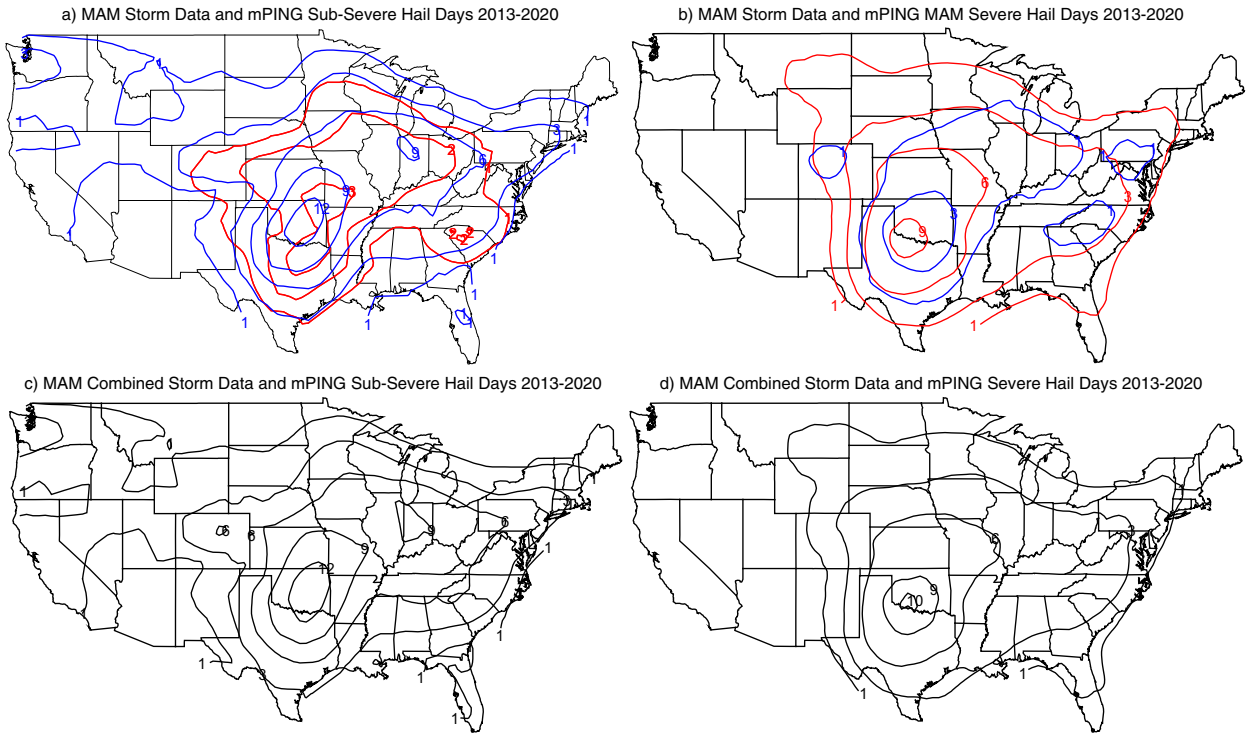

FIG. 7. (a) Contours of spring (March, April, May) average number of sub-severe hail days from *Storm Data* (red) and mPING (blue). (b) As in (a), but for the spring average number of severe hail days. (c) Contours spring average number of sub-severe hail days in spring from both *Storm Data* and mPING combined. (d) As in (c), but for the spring average number of severe hail days.

however, they also illustrate further regional detail and local maxima.

It is well established that hail displays a strong seasonal cycle with regional variation perhaps even more so than tornado frequency (Changnon 1977a,b; Doswell et al. 2005; Changnon et al. 2009; Allen and Tippett 2015; Taszarek et al. 2020). To explore these distributions in terms of both sub-severe and severe hail, we explore these characteristics using the seasons as defined from the National Centers for Environmental Prediction, spring (March, April, May), summer (June, July, August), fall (September, October, November), and winter (December, January, February), hereafter MAM, JJA, SON, and DJF, respectively.

Springtime yields the highest frequency for both sub-severe and severe hail over the central Plains (Fig. 7). This broadly consistent with station-based estimates in earlier climatologies (Changnon et al. 2009). *Storm Data* in contrast produces only about three days of sub-severe hail during an average spring (Fig. 7a), in a rough ellipse extending from northeast Texas across eastern Oklahoma, into southwestern Missouri including the southeast corner of Kansas. Because of *Storm Data* constraints and aforementioned properties this undercount is expected. The mPING average number of spring sub-severe hail days capture generally the same spatial pattern for the highest values, but the number of days increase substantially. Higher frequencies also more broadly extend into the Midwest, and minimum contours are more expansive than those of *Storm Data*. Merging the two sources (Fig. 7c) the pattern is driven primarily by mPING observations. This yields a maximum of ~13 days of sub-severe hail observations situated over east central Oklahoma, extending up into the Great Lakes region then eastward into southern New England. There is another maximum (6 days) nestled into the Denver area. For severe hail (Figs. 8c,b), *Storm Data* days are again more numerous that mPING observations. Here we see maximum average number of days (~9 days) shifted slightly to the west and south from the sub-severe days, which is instead centered in southwest Oklahoma. A weak ridge of activity extends to the north and east, following roughly the same pattern as for sub-severe hail, but much attenuated. mPING severe hail days are remarkably similar to *Storm Data* observations, but with fewer observations outside of the traditional hail belt of Texas–Oklahoma–Kansas–Nebraska–Missouri. A nonmeteorological explanation for this focus may be a function of project familiarity in and around the central Oklahoma area. Finally, merging the two sources (Fig. 7d) the overall pattern is driven by the larger data source in *Storm Data*. The ridge of enhanced activity clearly delineates the expected "hail alley," along with a broad region of higher frequency extending to the Atlantic coast.

In the summer, sub-severe hail shifts northward with a broad axis extending from the Rocky Mountains through the Midwest (Fig. 8a). Higher frequencies also extend into the southeastern United States, reflecting weakly forced pulse storms during the summer in this region (Miller and Mote 2017). *Storm Data* generally undercounts sub-severe hail days, and the pattern is

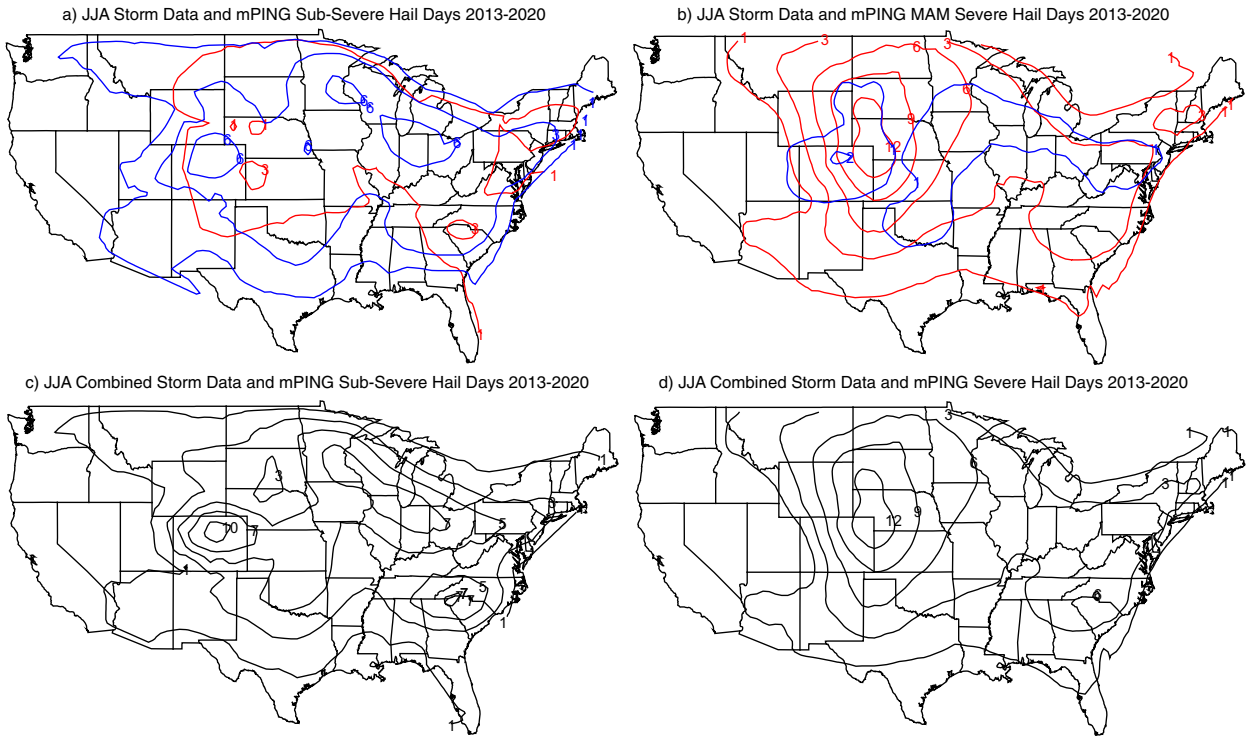

FIG. 8. (a) Contours of the yearly average number of sub-severe hail days in summer from *Storm Data* (red) and mPING (blue). (b) As in (a), but for severe hail. (c) Contours of the yearly average number of sub-severe hail days in summer from both *Storm Data* and mPING combined. (d) As in (b), but for severe hail.

significantly different from spring, while mPING sub-severe hail days provide a more coherent depiction. The maximum of 8 days is found in the Denver/Ft. Collins, Colorado, area, an extended area of 6–7 days from eastern Minnesota, through the Chicago, Illinois, area and then through Pennsylvania. Again, by merging the two data sources (Fig. 8c), we see a more complete picture, with a weak maximum remaining in central Oklahoma, the orographically driven maximum over the Denver area extending into eastern Colorado is clearly evident, as is a band of hail activity from eastern Minnesota through the lower Great Lakes and into New England, and a separate maximum is found over the southeast. When only *Storm Data* severe hail is considered (Fig. 8b), the maximum frequency is clearly centered over northeastern Colorado and extends north into western South Dakota, with a broad band of high frequency across the Midwest into the mid-Atlantic. Combining the two datasets results in a broader range of higher frequency severe hail, extending into the northeast (Fig. 8d).

To better illustrate the seasonal progression of occurrence Fig. 9 shows the total hail days, regardless of size, across the seasons from both sources. The average number of winter days with any hail is as would be expected low given limited instability (Fig. 9d). A broad maximum during this season is found over eastern Texas, southeastern Oklahoma, Arkansas, northern Louisiana, and southern Missouri. This hints at the maximum in severe weather frequency over the southeast CONUS. Also, on average at least 1 day of hail occurs along the West Coast, with 2 days on average in western Washington. Frequency rapidly increases into the spring months, with a strong Great Plains signal that extends into the Denver, Colorado, area. Spring, however, is early in the hail season for many areas closer to the mountains and through the Midwest and Northeast. During summer maximum surface heating along with convection reach their peak. Two very distinct maxima are identified during the summer for any hail day: one over the Denver area (likely associated with topographic forcing, the "Denver cyclone" (Wilczak and Glendening 1988) and the southwest monsoon), and a second maximum over the western North Carolina. The belt of 7–8 days of hail extending from eastern Minnesota around the Great Lakes through Pennsylvania becomes more diffuse, but is still evident. Fall sees waning frequency and a lower overall number of days with hail (Fig. 9c). Only 3 days of hail of any size occur and these days all contain a mix of sub-severe and severe hail. On average a broad area of two severe hail days is centered on the Kansas–Nebraska border (not shown). The main area of hail activity extends from central Oklahoma into Iowa, then eastern Minnesota, curving around the Great Lakes into far western Pennsylvania.

Another viewpoint for the seasonal cycle is to consider monthly snapshots through its progression, from March to May and July (Fig. 10). In March a broad area of severe hail overlays the southeastern CONUS, evidence of the southeastern maximum in severe weather frequency. The number of average severe hail days for May increases, displaying a clear

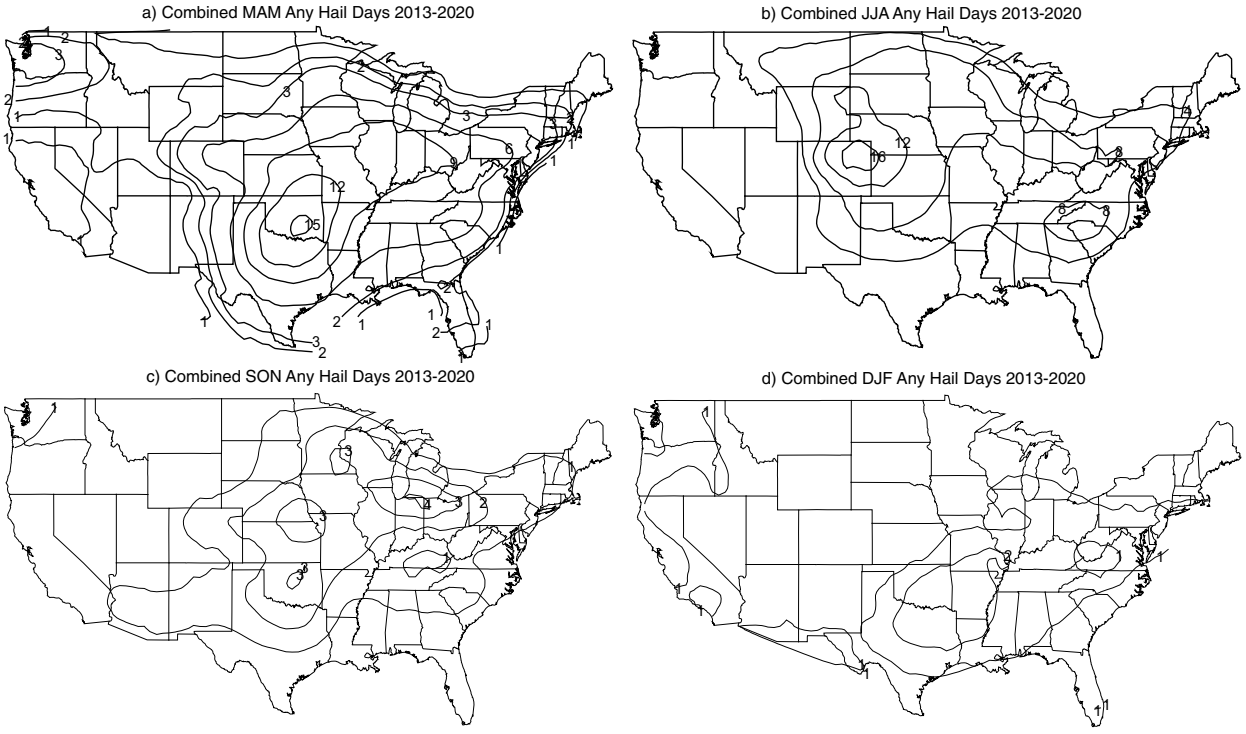

FIG. 9. (a) Contours of the spring average number of days with any hail regardless of size from *Storm Data* and mPING combined regardless of hail size. (b) As in (a), but for the summer months (June, July, August). (c) As in (a), but for the fall months (September, October, November). (d) As in (a), but for the winter (December, January, February).

maximum over western Oklahoma and the eastern Texas Panhandle. By July, the frequency maximum extends over the northeast panhandle. As has been shown in prior research, the area of peak severe weather progresses west and north from March through July.

b. *Hail size distribution*

Given the distinct differences in the number of sub-severe and severe hail reports between the datasets, a broader examination of the hail size distribution may reveal how these datasets capture the distribution of hail sizes from all reported instances. All reported hail sizes are rounded to the nearest 6.35 mm (0.25 in.), and a kernel density estimate (KDE) across 201 points using a Gaussian weight 12.7 mm (0.5 in.) wide truncated at four standard deviations (KDEs; Silverman 1998) of the hail size probability density function estimated. For completeness, the approach here also considers the hail size distribution from CoCoRaHS reports in comparison to the other two datasets. Figure 11 displays the hail size pdfs from all three sources; the missing small sizes are readily apparent in *Storm Data*. This problematic size distribution has been discussed in prior literature (Allen and Tippett 2015; Allen et al. 2017), with the added influence of clear discontinuities in the pdf associated with the minimum size threshold (0.75 in.), but also the common reference objects used (25.4 mm or 1 in., 45 mm or 1.75-in. golf ball, 70 mm or 2.75-in. baseball). In comparison, both CoCoRAHS and mPING show a more continuous distribution that includes the smaller sizes, reflecting a more even weighting of frequency toward these categories. Owing to the challenges of *Storm Data* for understanding the characteristic hail size pdf, we consider a combined pdf of CoCoRaHS and mPING size data (Fig. 11). Contrasting the *Storm Data* pdf, sizes less than 25.4 mm (1 in.) comprise nearly 95% of all the 95 009 hail reports (15 169 from CoCoRahs and 79 840 from mPING). This suggests that the use of mPING and CoCoRaHS data combined is a realistic approach to offset the size biases inherent in *Storm Data*, and these datasets now constitute a record to better explore the occurrence of sub-severe hail and complement the larger sample size of *Storm Data*. We do, however, note that CoCoRaHS data may be biased small, as

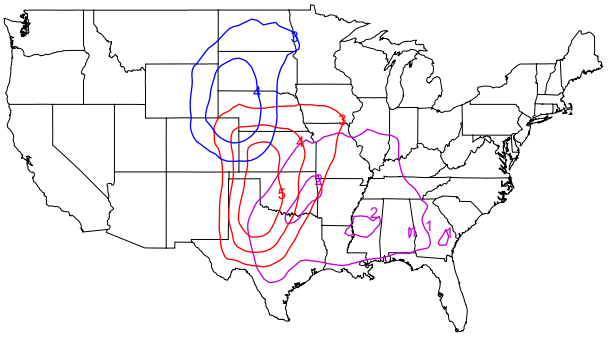

FIG. 10. Contours of the yearly average number days with severe hail for monthly snapshots to illustrate the seasonal cycle in March (purple), May (red), and July (blue).

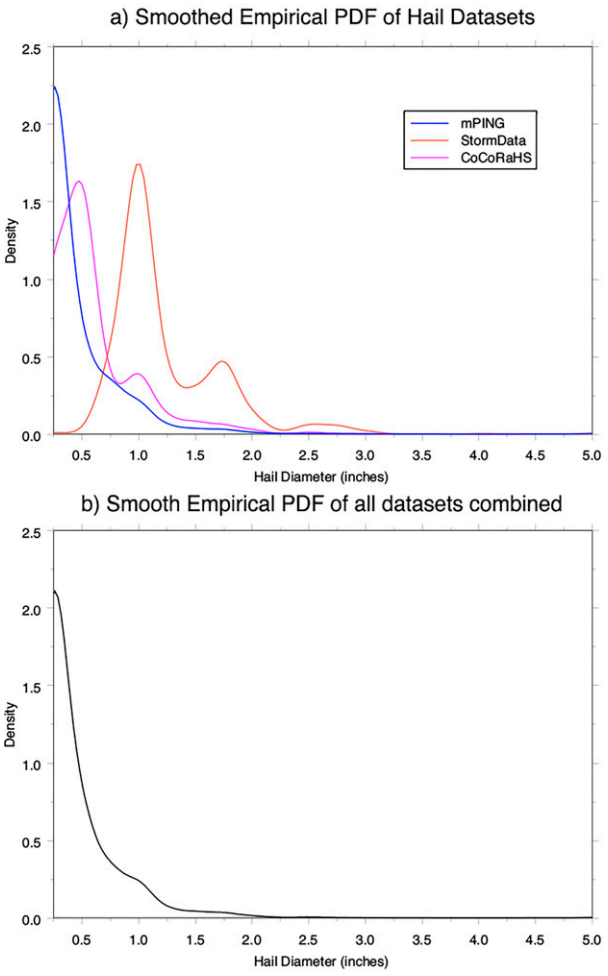

FIG. 11. (a) KDE pdfs of hail size for *Storm Data* (red), mPING (blue), and CoCoRaHS (purple). (b) KDE pdfs using combined mPING and CoCoRaHS data.

it allows reporting of much smaller sizes leading to differences in the eCDF which imply preferred sizes reported within CoCORaHS that do not appear in mPING. It is also likely that to some extent mPING data may be biased large because the hail size is estimated rather than measured, and the maximum reporting size of 127 mm (5 in.) may influence the overall pdf.

c. *Occurrence times*

A final climatological aspect of interest is the relative time of occurrence (Fig. 12a). Transforming hail occurrence time of any size across the respective seasons to LST and applying a KDE (Silverman 1998), allows exploration of how the temporal structure of hail occurrence varies. We note here that *Storm Data* occurrence times may on occasion be biased toward later in the day due to observer bias, especially if the occurrence time is estimated, and possibly by errors in recording the observation time itself, i.e., recording the submission time rather than the observation time. Even so we expect such errors

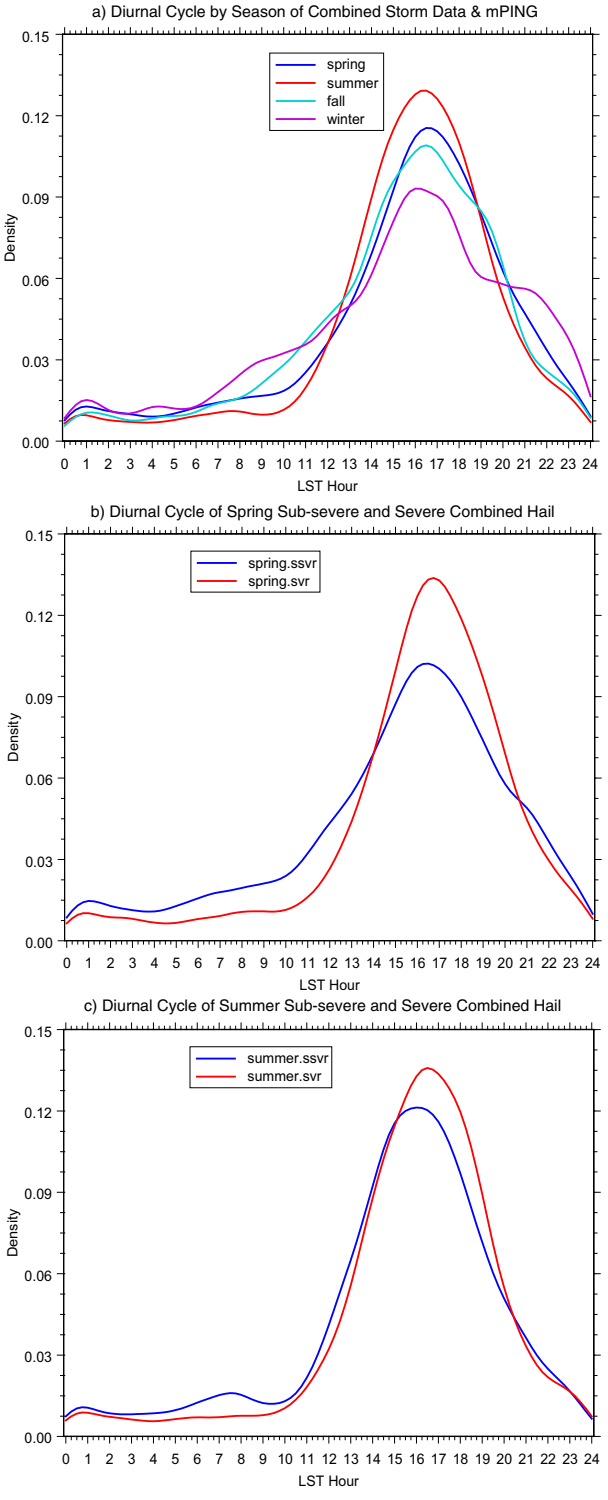

FIG. 12. (a) Report/occurrence time in LST of *Storm Data* and mPING hail events for spring (blue), summer (red), fall (cyan), and winter (magenta). (b) Kernel density estimates of report/occurrence times for *Storm Data* and mPING spring severe hail (red) and sub-severe hail (blue). (c) As in (b), but for summer severe (red) and sub-severe (blue).

to be rare enough that they do not affect the overall results of the larger sample. All seasons show peaks in the late afternoon with relatively slight variations: spring at 1630 LST, summer at 1615 LST, fall at 1615 LST, and winter at 1600 LST. These times bracket the peak convective periods that usually follow daytime heating. Variations away from these peaks and spreading of the times away from these peaks may indicate additional effects due to synoptic-scale dynamic processes, a signal highlighted by the higher relative frequencies outside of this peak in winter.

Seasonally, there are small but discernible differences between the peak times for sub-severe and severe hail (Fig. 12). Two characteristics stand out: the sub-severe peak is at 1630 LST while the severe peak is on average later in the day at 1645 LST, and the sub-severe peak is more broad than the severe peak is. This is physically consistent as severe hail comes from more energetic convection that likely occurs later in the day in response to greater diabatic heating and the capping inversion's delay of convection. Sub-severe hail report times are more spread out, possibly indicating that while the convection is strong enough to produce hail, these storms reflect a greater fraction of weakly forced or pulse storms (Miller and Mote 2017), or time frames when convection has weaker vertical updrafts, both earlier in the day and after the nocturnal transition. Differences in the summer are similar: peak report time for sub-severe hail is 1600 LST while peak report time for severe hail is 1630 LST. The difference is more pronounced and likely reflects the contribution of orographic initiation of thunderstorms earlier in the day, or regions where air mass thunderstorms are more common but still indicates that the severe reports come later in the day. This also implies that generally speaking sub-severe hail is generated on the periphery of severe convection or to its exclusion.

4. Discussion

The exploration of datasets here illustrates that one hail dataset is not superior to another, but rather they approach the characterization of hail occurrence from alternative perspectives and different purposes. In this way, we suggest that the data comprising *Storm Data* and mPING are complimentary in nature. Through playing to these dataset's relative strengths, we are able to capture a more holistic picture of the hail hazard, similar to the opportunities afforded by station reported records (Changnon and Changnon 2000). By its very design and implementation, *Storm Data* is clearly the better dataset if the goal is to capture severe hail days. While mPING data expands somewhat on severe hail day numbers, its primary strength is that it provides a more detailed depiction of smaller, sub-severe hail sizes that *Storm Data* is not designed to capture. *Storm Data* is clearly the better dataset if the goal is to capture severe hail days, while mPING data expands on severe hail day numbers, but also provides a more detailed depiction of smaller subsevere hail sizes. There are other advantages and disadvantages to the respective datasets as well. mPING reflects a true volunteer and passive collection dataset, capturing whatever observers report. In contrast, *Storm Data* is biased because in addition to such voluntary reports, the NWS Weather Forecast Offices (WFOs) actively search for severe hail reports (as well as other events) as an approach to verify severe weather warnings (Blair et al. 2011; Bunkers et al. 2020). This can lead to an under-sampling bias, or a bias toward the larger hail size as the NWS does not continue probing once a warning has been verified (Ortega et al. 2009). Similar to Allen and Tippett (2015), by approaching hail days rather than reports or individual hail events the results presented here are largely unaffected by this characteristic. Curiously, despite relatively widespread coverage mPING severe hail data appears to be a subsample of *Storm Data*. It is true that *Storm Data* may record sub-severe hail events, but usually this is as an adjunct to some other significant weather event, and since the change of severe criteria in 2010 to 25.4 mm (1 in.), these reports have decreased in frequency (Allen and Tippett 2015). Despite the differences in the total frequency of reports, it is clear that both sources tend to capture similar patterns.

While hail, even severe hail, has a relatively common rate of occurrence across the United States it is not commonly observed because of its temporal and spatial heterogeneity and the need to have an observer present (Allen and Tippett 2015). There is no reason to suspect that mPING observers are censoring observations of severe hail, especially since both mPING and *Storm Data* tend to capture similar spatial patterns, though mPING captures fewer days of severe hail. The likely explanation for this disparity is that the density of mPING observers is not as widespread or as high as the potential sources of reports for *Storm Data*, both volunteer and solicited. Despite *Storm Data* not aiming to collect sub-severe hail, there are also pattern similarities that raise an important question about the sub-severe hail days. As mPING is passive, we note that it tends to miss severe hail events by a factor of 3–5 in comparison to *Storm Data*. This leads the authors to speculate: is mPING missing the non-severe hail events by the same ratio? If so, the count of sub-severe hail days may be too low by a factor of at least 3. Also, within mPING non-severe hail often (but not always) accompanies severe hail observations, though there are clearly days and places when no severe hail is reported but sub-severe hail is. In all likelihood, it is likely that the spatial distribution here underrepresents the frequency of sub-severe hail days, yet the overall pattern of sub-severe hail occurrence is likely well captured. Through analysis and comparison of the sub-severe and severe hail distributions to date using these data, we illustrate that sub-severe hail does not always mimic severe hail.

While spatial properties retain some limitations from the sampling, we can ascribe greater confidence for the hail size eCDFs and analysis of hail report times. Both of these metrics are less sensitive to the heterogeneity that can create problems with finding the days with hail. Hail size pdfs indicate that slightly less than 5% of the hail that has been observed over the 8 years covered by mPING here meets severe criteria. The remaining record is sub-severe, suggesting that greater attention needs to be paid to exploring how to represent hail days beyond arbitrary severe hail criteria (Doswell 2001), as sub-severe hail can still be damaging to agriculture or lead to large accumulations (Kumjian et al. 2019; Friedrich et al. 2019) that can cause dangerous road conditions and exacerbate flash floods. The diurnal nature of hail reports unsurprisingly leads to an afternoon peak, though clearly if the goal

is to sample sub-severe hail, a broader period of observation is necessary.

5. Conclusions

Data from three sources (*Storm Data*, CoCoRaHS, and mPING) over the past 8 years have been used to construct a more complete climatology of hail days and characteristics over the CONUS. Differences between these data sources have been discussed to illustrate their relative strengths and applicability, both in combination and individually. Seasonal differences in number of hail days and their spatial distributions have been illustrated, with a spring and summer peak of frequency with a shift of peak from the southeastern CONUS into the northwestern plains, more so than seen in only severe hail data. Considering sub-severe hail days (days with hail less than 25.4 mm in diameter) and severe hail days, we have shown that there are notable differences in the peaks of hail climatology. Severe hail days also generally record sub-severe hail somewhere, suggesting that the two datasets are not independent. Yet, the spatial distribution of sub-severe hail days differs markedly in some cases from severe hail days.

Considering the reasons for these different depictions, we also explore the size distribution of observed hail through the use of CoCoRaHS, mPING, and *Storm Data* reports. As mPING and CoCoRaHS offer more distributionally complete representations of hail size, we present a combined eCDF that illustrates the utility of these data to explore the relationship of hail size at the ground to remotely sensed characteristics.

For environmental studies, or other approaches that rely on the time of occurrence we highlighted the distribution of hail in terms of LST. This analysis reveals differences between sub-severe and severe hail occurrence of 30 min to 1 h, which is much larger than that between seasons, suggesting that care should be taken when selecting a proximal profile if considering sub-severe hail environments.

While this work follows on from the depiction of hail occurrence from prior studies (e.g., Kelly et al. 1985; Schaefer et al. 2004; Doswell et al. 2005; Allen and Tippett 2015; Taszarek et al. 2020), it provides a novel insight into the voluntarily sourced small, or sub-severe hail, which has not been directly examined with size information in prior work outside of isolated field datasets. This difference also means that through the use of datasets such as mPING or CoCoRaHS a more comprehensive depiction of hail size distributions is now available to the community. As these datasets continue to grow, this will likely provide a more comprehensive viewpoint of hail occurrence for all sizes offering better opportunities for the validation of radar hail detection, similar to the saturation seen in equivalent approaches in Switzerland (Barras et al. 2019).

Despite the advantages, and combination of datasets, the challenges and limitations with observational data remain. Both mPING and CoCoRaHS suffer from the same problems that afflict all other similar observational studies: the uneven spatial distribution of observations. Changnon (1999) pointed to the advantage of fixed station observers for deriving hail frequency, which is that, generally speaking, these stations reliably identified any hail occurrence in their vicinity. To some extent, this is somewhat less of a problem within *Storm Data*, particularly in more populated areas of the country, since if no report is received in an area warned for a severe thunderstorm, the NWS WFOs actively probe for verifying observations. The challenge to uncovering a true climatology is that uneven spatial observation distribution cannot be solved by a longer period of record if observations are normalized by area or days as is done here and in other similar studies. The only solution for this problem is to have more observations across a wider array of locations and users. The impacts of spatial inhomogeneity are most easily seen in the difference between the spatial distribution of *Storm Data* severe hail days as compared to mPING severe hail days. Usually, *Storm Data* has at least 3 times the number of severe hail days that mPING reports, sometimes more. This difference implies that as diligent as mPING observers are, small hail is probably missed at about the same rate that large hail is missed. Thus, we suspect that there are overall probably 3 times as many sub-severe hail days as seen here. While the spatial patterns of sub-severe hail days are likely correct, the frequency remains underestimated.

To offset these limitations remotely sensed climatologies of estimated hail occurrence are now possible (e.g., Cintineo et al. 2012; Murillo et al. 2021; Wendt and Jirak 2021). These technologies are available over a near complete spatiotemporal range for the continent outside of the western CONUS. However, these approaches focus strongly on the maximum expected size of hail, and through lack of appropriate validation data, generally leave sub-severe hail as an afterthought, despite its societal implications. Despite the efforts of projects such as SHAVE (Ortega et al. 2009; Ortega 2018), or those in Switzerland (Barras et al. 2019) a greater volume of sub-severe hail reports is needed to understand the best approach to characterize the total frequency of hail days, the properties of smaller hailstones, and sub-severe hail economic impacts. The question of whether small hail occurrence has changed over time is also a reason to maintain and expand such datasets. For example, over both China and France there have been decreasing trends in smaller hail (Li et al. 2016; Sanchez et al. 2017), contrasting the stationary frequency or increases seen for larger hail in the United States (Allen et al. 2015; Tang et al. 2019). With climate projections indicating strong decreases to smaller hail, approaches are needed to monitor these events (Mahoney et al. 2012; Brimelow et al. 2017; Trapp et al. 2019). For mPING and CoCoRAHS to develop into this level of climatological resource likely means that the best approach into the future will be recruitment of additional observers as well as dedicated support. As the observer density increases, fewer events will "slip between the gaps."

Acknowledgments. Funding was provided for K. Elmore by NOAA/Office of Oceanic and Atmospheric Research under NOAA–University of Oklahoma Cooperative Agreement NA21OAR4320204, U.S. Department of Commerce. J. Allen acknowledges funding support from the National Science Foundation (AGS-1945286).

Data availability statement. Observational hail reports from the mPING data are available through an API request at https://mping.ou.edu/, with instructions provided for the structuring of requests. *Storm Data* reports for hail for the period can be freely obtained from the Storm Prediction Center https://www.spc.noaa.gov/wcm/. CoCoRaHS data are available from the project website and use of a web-API request https://www.cocorahs.org/ViewData/ListHailReports.aspx.

REFERENCES

Allen, J. T., and M. K. Tippett, 2015: The characteristics of United States hail reports: 1955–2014. *Electron. J. Severe Storms Meteor.*, **10**(3), https://ejssm.com/ojs/index.php/site/article/view/60.

——, ——, and A. H. Sobel, 2015: An empirical model relating U.S. monthly hail occurrence to large-scale meteorological environment. *J. Adv. Model. Earth Syst.*, **7**, 226–243, https://doi.org/10.1002/2014MS000397.

——, ——, Y. Kaheil, A. H. Sobel, C. Lepore, S. Nong, and A. Muehlbauer, 2017: An extreme value model for U.S. hail size. *Mon. Wea. Rev.*, **145**, 4501–4519, https://doi.org/10.1175/MWR-D-17-0119.1.

——, I. M. Giammanco, M. R. Kumjian, H. Jurgen Punge, Q. Zhang, P. Groenemeijer, M. Kunz, and K. Ortega, 2020: Understanding hail in the Earth system. *Rev. Geophys.*, **58**, e2019RG000 665, https://doi.org/10.1029/2019RG000665.

Bang, S. D., and D. J. Cecil, 2019: Constructing a multifrequency passive microwave hail retrieval and climatology in the GPM domain. *J. Appl. Meteor. Climatol.*, **58**, 1889–1904, https://doi.org/10.1175/JAMC-D-19-0042.1.

Barras, H., A. Hering, A. Martynov, P.-A. Noti, U. Germann, and O. Martius, 2019: Experiences with >50,000 crowdsourced hail reports in Switzerland. *Bull. Amer. Meteor. Soc.*, **100**, 1429–1440, https://doi.org/10.1175/BAMS-D-18-0090.1.

Blair, S. F., D. R. Deroche, J. M. Boustead, J. W. Leighton, B. L. Barjenbruch, and W. P. Gargen, 2011: A radar-based assessment of the detectability of giant hail. *Electron. J. Severe Storms Meteor.*, **6**(7), https://ejssm.com/ojs/index.php/site/issue/view/32.

——, and Coauthors, 2017: High-resolution hail observations: Implications for NWS warning operations. *Wea. Forecasting*, **32**, 1101–1119, https://doi.org/10.1175/WAF-D-16-0203.1.

Brimelow, J. C., W. R. Burrows, and J. M. Hanesiak, 2017: The changing hail threat over North America in response to anthropogenic climate change. *Nat. Climate Change*, **7**, 516–522, https://doi.org/10.1038/nclimate3321.

Brooks, H. E., J. W. Lee, and J. P. Craven, 2003: The spatial distribution of severe thunderstorm and tornado environments from global reanalysis data. *Atmos. Res.*, **67–68**, 73–94, https://doi.org/10.1016/S0169-8095(03)00045-0.

Brown, T. M., W. H. Pogorzelski, and I. M. Giammanco, 2015: Evaluating hail damage using property insurance claims data. *Wea. Climate Soc.*, **7**, 197–210, https://doi.org/10.1175/WCAS-D-15-0011.1.

Bunkers, M. J., S. R. Fleegel, T. Grafenauer, C. J. Schultz, and P. N. Schumacher, 2020: Observations of hail–wind ratios from convective storm reports across the continental United States. *Wea. Forecasting*, **35**, 635–656, https://doi.org/10.1175/WAF-D-19-0136.1.

Carr, D. B., A. R. Olsen, and D. White, 1992: Hexagon mosaic maps for display of univariate and bivariate geographical data. *Cartogr. Geogr. Info. Syst.*, **19**, 228–236, https://doi.org/10.1559/152304092783721231.

Cecil, D. J., and C. B. Blankenship, 2012: Toward a global climatology of severe hailstorms as estimated by satellite passive microwave imagers. *J. Climate*, **25**, 687–703, https://doi.org/10.1175/JCLI-D-11-00130.1.

Changnon, D., and S. A. Changnon, 1997: Surrogate data to estimate crop-hail loss. *J. Appl. Meteor.*, **36**, 1202–1210, https://doi.org/10.1175/1520-0450(1997)036<1202:SDTECH>2.0.CO;2.

——, ——, and S. S. Changnon, 2001: A method for estimating crop losses from hail in uninsured periods and regions. *J. Appl. Meteor. Climatol.*, **40**, 84–91, https://doi.org/10.1175/1520-0450(2001)040<0084:AMFECL>2.0.CO;2.

Changnon, S. A., 1971: Hailfall characteristics related to crop damage. *J. Appl. Meteor.*, **10**, 270–274, https://doi.org/10.1175/1520-0450(1971)010<0270:HCRTCD>2.0.CO;2.

——, 1977a: The climatology of hail in North America. *Hail: A Review of Hail Science and Hail Suppression*, G. B. Foote and C. A. Knight, Eds., Springer, 107–133.

——, 1977b: The scales of hail. *J. Appl. Meteor.*, **16**, 626–648, https://doi.org/10.1175/1520-0450(1977)016<0626:TSOH>2.0.CO;2.

——, 1999: Data and approaches for determining hail risk in the contiguous United States. *J. Appl. Meteor.*, **38**, 1730–1739, https://doi.org/10.1175/1520-0450(1999)038<1730:DAAFDH>2.0.CO;2.

——, and D. Changnon, 2000: Long-term fluctuations in hail incidences in the United States. *J. Climate*, **13**, 658–664, https://doi.org/10.1175/1520-0442(2000)013<0658:LTFIHI>2.0.CO;2.

——, ——, and S. D. Hilberg, 2009: Hailstorms across the nation: An atlas about hail and its damages. ISWS Contract Report CR-2009-12. Tech. Rep., Illinois State Water Survey, http://hdl.handle.net/2142/15156.

Cintineo, J. L., T. M. Smith, V. Lakshmanan, H. E. Brooks, and K. L. Ortega, 2012: An objective high-resolution hail climatology of the contiguous United States. *Wea. Forecasting*, **27**, 1235–1248, https://doi.org/10.1175/WAF-D-11-00151.1.

Cleveland, W. S., 1979: Robust locally weighted regression and smoothing scatterplots. *J. Amer. Stat. Assoc.*, **74**, 829–836, https://doi.org/10.1080/01621459.1979.10481038.

——, and S. J. Devlin, 1988: Locally weighted regression: An approach to regression analysis by local fitting. *J. Amer. Stat. Assoc.*, **83**, 596–610, https://doi.org/10.1080/01621459.1988.10478639.

Doswell, C. A., III, 2001: Severe convective storms—An overview. *Severe Convective Storms, Meteor. Monogr.*, No. 28, Amer. Meteor. Soc., 1–26, https://doi.org/10.1175/0065-9401-28.50.1.

——, H. E. Brooks, and M. P. Kay, 2005: Climatological estimates of daily local nontornadic severe thunderstorm probability for the United States. *Wea. Forecasting*, **20**, 577–595, https://doi.org/10.1175/WAF866.1.

Elmore, K. L., Z. Flamig, V. Lakshmanan, B. Kaney, V. Farmer, H. D. Reeves, and L. P. Rothfusz, 2014: mping: Crowd-sourcing weather reports for research. *Bull. Amer. Meteor. Soc.*, **95**, 1335–1342, https://doi.org/10.1175/BAMS-D-13-00014.1.

Friedrich, K., and Coauthors, 2019: CHAT: The Colorado Hail Accumulation from Thunderstorms Project. *Bull. Amer. Meteor. Soc.*, **100**, 459–471, https://doi.org/10.1175/BAMS-D-16-0277.1.

Gensini, V. A., A. M. Haberlie, and P. T. Marsh, 2020: Practically perfect hindcasts of severe convective storms. *Bull. Amer. Meteor. Soc.*, **101**, E1259–E1278, https://doi.org/10.1175/BAMS-D-19-0321.1.

Giammanco, I. M., B. R. Maiden, H. E. Estes, and T. M. Brown-Giammanco, 2017: Using 3D laser scanning technology to create digital models of hailstones. *Bull. Amer. Meteor. Soc.*, **98**, 1341–1347, https://doi.org/10.1175/BAMS-D-15-00314.1.

Grieser, J., and M. Hill, 2019: How to express hail intensity—Modeling the hailstone size distribution. *J. Appl. Meteor. Climatol.*, **58**, 2329–2345, https://doi.org/10.1175/JAMC-D-18-0334.1.

Kacan, K. G., and Z. J. Lebo, 2019: Microphysical and dynamical effects of mixed-phase hydrometeors in convective storms using a bin microphysics model: Melting. *Mon. Wea. Rev.*, **147**, 4437–4460, https://doi.org/10.1175/MWR-D-18-0032.1.

Kelly, D. L., J. T. Schaefer, and C. A. Doswell III, 1985: Climatology of nontornadic severe thunderstorm events in the United States. *Mon. Wea. Rev.*, **113**, 1997–2014, https://doi.org/10.1175/1520-0493(1985)113<1997:CONSTE>2.0.CO;2.

Kumjian, M. R., Z. J. Lebo, and A. M. Ward, 2019: Storms producing large accumulations of small hail. *J. Appl. Meteor. Climatol.*, **58**, 341–364, https://doi.org/10.1175/JAMC-D-18-0073.1.

Li, M., Q. Zhang, and F. Zhang, 2016: Hail day frequency trends and associated atmospheric circulation patterns over China during 1960–2012. *J. Climate*, **29**, 7027–7044, https://doi.org/10.1175/JCLI-D-15-0500.1.

Mahoney, K., M. A. Alexander, G. Thompson, J. J. Barsugli, and J. D. Scott, 2012: Changes in hail and flood risk in high-resolution simulations over Colorado's mountains. *Nat. Climate Change*, **2**, 125–131, https://doi.org/10.1038/nclimate1344.

Miller, P. W., and T. L. Mote, 2017: A climatology of weakly forced and pulse thunderstorms in the Southeast United States. *J. Appl. Meteor. Climatol.*, **56**, 3017–3033, https://doi.org/10.1175/JAMC-D-17-0005.1.

Murillo, E. M., C. R. Homeyer, and J. T. Allen, 2021: A 23-year severe hail climatology using GridRad MESH observations. *Mon. Wea. Rev.*, **149**, 945–958, https://doi.org/10.1175/MWR-D-20-0178.1.

Ortega, K. L., 2018: Evaluating multi-radar, multi-sensor products for surface hailfall diagnosis. *Electron. J. Severe Storms Meteor*, **13**(1), https://ejssm.com/ojs/index.php/site/issue/view/66.

——, T. M. Smith, K. L. Manross, K. A. Scharfenberg, A. Witt, A. G. Kolodziej, and J. J. Gourley, 2009: The Severe Hazards Analysis And Verification Experiment. *Bull. Amer. Meteor. Soc.*, **90**, 1519–1530, https://doi.org/10.1175/2009BAMS2815.1.

Reges, H. W., N. Doesken, J. Turner, N. Newman, A. Bergantino, and Z. Schwalbe, 2016: CoCoRaHS: The evolution and accomplishments of a volunteer rain gauge network. *Bull. Amer. Meteor. Soc.*, **97**, 1831–1846, https://doi.org/10.1175/BAMS-D-14-00213.1.

Sanchez, J., A. Merino, P. Melcón, E. García-Ortega, S. Fernández-González, C. Berthet, and J. Dessens, 2017: Are meteorological conditions favoring hail precipitation change in Southern Europe? Analysis of the period 1948–2015. *Atmos. Res.*, **198**, 1–10, https://doi.org/10.1016/j.atmosres.2017.08.003.

Sander, J., J. Eichner, E. Faust, and M. Steuer, 2013: Rising variability in thunderstorm-related U.S. losses as a reflection of changes in large-scale thunderstorm forcing. *Wea. Climate Soc.*, **5**, 317–331, https://doi.org/10.1175/WCAS-D-12-00023.1.

Schaefer, J. T., J. J. Levit, S. J. Weiss, and D. W. McCarthy, 2004: The frequency of large hail over the contiguous United States. *14th Conf. on Applied Climatology*, Seattle, WA, Amer. Meteor. Soc., 3.3, https://ams.confex.com/ams/84Annual/techprogram/paper_69834.htm.

Silverman, B. W., 1998: *Density Estimation for Statistics and Data Analysis.* Routledge, 176 pp.

Tang, B. H., V. A. Gensini, and C. R. Homeyer, 2019: Trends in United States large hail environments and observations. *npj Climate Atmos. Sci.*, **2**, 45, https://doi.org/10.1038/s41612-019-0103-7.

Taszarek, M., J. T. Allen, P. Groenemeijer, R. Edwards, H. E. Brooks, V. Chmielewski, and S.-E. Enno, 2020: Severe convective storms across Europe and the United States. Part I: Climatology of lightning, large hail, severe wind, and tornadoes. *J. Climate*, **33**, 10 239–10 261, https://doi.org/10.1175/JCLI-D-20-0345.1.

Trapp, R. J., K. A. Hoogewind, and S. Lasher-Trapp, 2019: Future changes in hail occurrence in the United States determined through convection-permitting dynamical downscaling. *J. Climate*, **32**, 5493–5509, https://doi.org/10.1175/JCLI-D-18-0740.1.

Van Den Heever, S. C., and W. R. Cotton, 2004: The impact of hail size on simulated supercell storms. *J. Atmos. Sci.*, **61**, 1596–1609, https://doi.org/10.1175/1520-0469(2004)061<1596:TIOHSO>2.0.CO;2.

Wendt, N. A., and I. L. Jirak, 2021: An hourly climatology of operational MRMS MESH-diagnosed severe and significant hail with comparisons to *Storm Data* hail reports. *Wea. Forecasting*, **36**, 645–659, https://doi.org/10.1175/WAF-D-20-0158.1.

Wilczak, J. M., and J. W. Glendening, 1988: Observations and mixed-layer modeling of a terrain-induced mesoscale gyre: The Denver cyclone. *Mon. Wea. Rev.*, **116**, 1599–1622, https://doi.org/10.1175/1520-0493(1988)116<1599:OAMLMO>2.0.CO;2.

Witt, A., M. D. Eilts, G. J. Stumpf, E. D. W. Mitchell, J. Johnson, and K. W. Thomas, 1998: Evaluating the performance of WSR-88D severe storm detection algorithms. *Wea. Forecasting*, **13**, 513–518, https://doi.org/10.1175/1520-0434(1998)013<0513:ETPOWS>2.0.CO;2.